

Article

Liquid Crystal Spatial Light Modulator with Optimized Phase Modulation Ranges to Display Multiorder Diffractive Elements

Elisabet Pérez-Cabré *  and María Sagrario Millán 

Departament d'Òptica i Optometria, Universitat Politècnica de Catalunya, Violinista Vellsolà 37, 08222 Terrassa, Spain

* Correspondence: elisabet.perez@upc.edu; Tel.: +34-93-739-8782

Received: 13 May 2019; Accepted: 19 June 2019; Published: 26 June 2019



Abstract: A liquid crystal on silicon spatial light modulator (LCoS SLM) with large phase modulation has been thoroughly characterized to operate optimally with several linear phase modulation ranges (π , 2π , 3π , 4π , 6π , and 8π) for an intermediate wavelength of the visible spectrum ($\lambda_G = 530$ nm). For each range, the device response was also measured for two additional wavelengths at the blue and red extremes of the visible spectrum ($\lambda_B = 476$ nm and $\lambda_R = 647$ nm). Multiorder diffractive optical elements, displayed on the LCoS SLM with the appropriate phase modulation range, allowed us to deal with some widely known encoding issues of conventional first-order diffractive lenses such as undersampling and longitudinal chromatic aberration. We designed an achromatic multiorder lens and implemented it experimentally on the SLM. As a result, the residual chromatic aberration reduces to one-third that of the chromatic aberration of a conventional first-order diffractive lens.

Keywords: liquid crystal spatial light modulator; liquid crystal on silicon device; phase characterization; phase modulation; diffractive optical element; multiorder diffractive lens; harmonic lens; chromatic aberration; aberration compensation; achromatic lens

1. Introduction

Diffractive optical elements (DOEs) have general advantages in comparison to their refractive counterparts such as being basically flat, thin, lightweight, and inexpensive when mass-produced. However, they exhibit large chromatic aberration (e.g., in diffractive lenses, approximately one diopter of axial chromatic aberration for every three diopters of power) and frequently low diffraction efficiency [1]. Sweeney and Sommargren [1] and Faklis and Morris [2] simultaneously and independently introduced DOEs with multiwavelength optical path-length transitions between adjacent facets, called harmonic and multiorder diffractive lenses, respectively. These lenses have hybrid properties of both refractive and diffractive lenses, and they have a common focus for a number of discrete wavelengths. Sweeney and Sommargren [1] measured the modulation transfer function (MTF) when a harmonic diffractive lens was used for imaging under either monochromatic or white light illumination. They showed that a lens with 10 wavelength phase steps approached diffraction limit behavior across the visible spectrum. Faklis and Morris [2] used multiorder diffractive lenses to design an achromatic diffractive singlet. The performance of such a lens was illustrated through MTF and Strehl ratio measurements as a function of wavelength. By 1995, advances in fabrication techniques of diffractive elements allowed development of the ideas proposed in these works. Multiorder DOEs have some constraints though. For example, higher-order structures restrain their off-axis performance. Because of the greater height at the edges of each facet, an effect appears, referred to as shadowing [3,4]. Even for diffraction angles of a few degrees, the wavefront emerging from the blazed structure has small gaps introduced by the

facets that affect the diffraction efficiency of the DOE [4]. This inconvenience can be overcome with the modern technology of liquid crystal (LC) displays.

The evolution of diffractive components experienced a significant advancement with the development of electrically addressed liquid crystal spatial light modulators (LC-SLM), capable of implementing a variety of programmable DOEs. Phase-only LC-SLM with a phase modulation depth larger than 2π radians is nowadays commercially available based on LC on silicon (LCoS) technology working on a reflection regime. A parallel-aligned LCoS display reaching a dynamic phase range of 4π radians for $\lambda = 454$ nm has been used to implement second-order diffraction DOEs, such as diffractive gratings and diffractive lenses, with some advantages in terms of resolution and diffraction efficiency compared to conventional first-order DOEs [5]. An LCoS-SLM initially designed to operate in infrared provides unusually large phase modulation depths in the visible band range, for instance, from 6π radians in the red region to 10π radians in the blue region [6]. This performance allows the display of a blazed diffractive grating with a reduced chromatic dispersion.

The discrete pixel structure [7] and the quantization of the available phase levels [8] of LC-SLM introduce some limitations in the implementation of DOEs on such displays. The spatial resolution of the screen may limit efficient encoding of diffractive lenses. On the one hand, low-resolution lenses implemented in the pixelated structure of LC-SLM introduce an inherent apodizing effect on the system point spread function (PSF). Apodization diminishes the secondary maxima of the PSF, but it increases the width of the central lobe [9,10]. These effects become more severe as the width of the pixel increases or as the focal length of the lens decreases. However, novel LCoS displays with a smaller pixel size and larger fill factor reduce the apodizing effect of the pixelated structure as they better approach the ideal continuous lens function. On the other hand, for diffractive lenses of low f-number, the facets become denser at the boundary of the lens aperture so the resolution needed to encode them may exceed the Nyquist frequency of the pixels on the LC-SLM [7]. To avoid aliasing of the lens function at the periphery, the design focal length f of the diffractive lens must meet the condition $f_N < f < 50f_N$, where the inferior limit f_N is the Nyquist focal length defined in [7,11].

In this paper, we present experimental results for multiorder diffractive lenses implemented in a parallel-aligned LCoS from Holoeye that reaches up to an 8π phase modulation range in the green region of the visible spectrum. To this end, we thoroughly characterize the device to optimize the setting parameter selection so as to obtain various linear operating phase modulation ranges (π , 2π , 3π , 4π , 6π , and 8π) for an intermediate wavelength of the visible spectrum ($\lambda_G = 530$ nm). Multiorder diffractive lenses with multiwavelength jumps at the edge of their facets permit to implement, on the LCoS device, higher optical power lenses with their focal length below the Nyquist focal length. These multiorder diffractive lenses overcome the aliasing effects that encoding of common first-order diffractive lenses have. An extended characterization of the LCoS display is carried out by determining the experimental phase modulation not only for the design wavelength, $\lambda_G = 530$ nm, but also for two additional wavelengths at the extremes of the visible spectrum ($\lambda_B = 476$ nm and $\lambda_R = 647$ nm). Based on the measured chromatic performance of the LCoS screen, we design an achromatic diffractive lens that operates with higher diffraction orders. We take advantage of the larger phase depth modulation of recently available parallel-aligned LCoS modulators to implement these DOEs in such a device with the additional benefits of real-time reprogramming and no shadowing effects. Moreover, further studies of the optical properties of multiorder diffractive lenses can be conducted without the need for physically manufacturing them.

We provide the experimental results for two multiorder lenses that overcome the issue of displaying a diffractive lens of optical power beyond the Nyquist interval and an achromatic diffractive lens. We compare their performances with that of a conventional, first-order diffractive lens.

2. Multiorder Diffractive Lenses: Theoretical Background

Multiorder diffractive lenses [1–4] are commonly built so that the optical path difference (OPD) at the boundaries of adjacent zones is a multiple of λ_0 , (or equivalently, a phase jump multiple of 2π rad).

Thus, $OPD = (f_0 + jq\lambda_0) - [f_0 + (j - 1)q\lambda_0] = q\lambda_0$ (Figure 1), where λ_0 is the design wavelength, f_0 is the focal length when the illumination wavelength is $\lambda = \lambda_0$, and q is an integer that multiplies 2π at the phase jump. A conventional diffractive lens with facets reaching 2π phase variation (also called a modulo 2π lens) has $q = 1$.

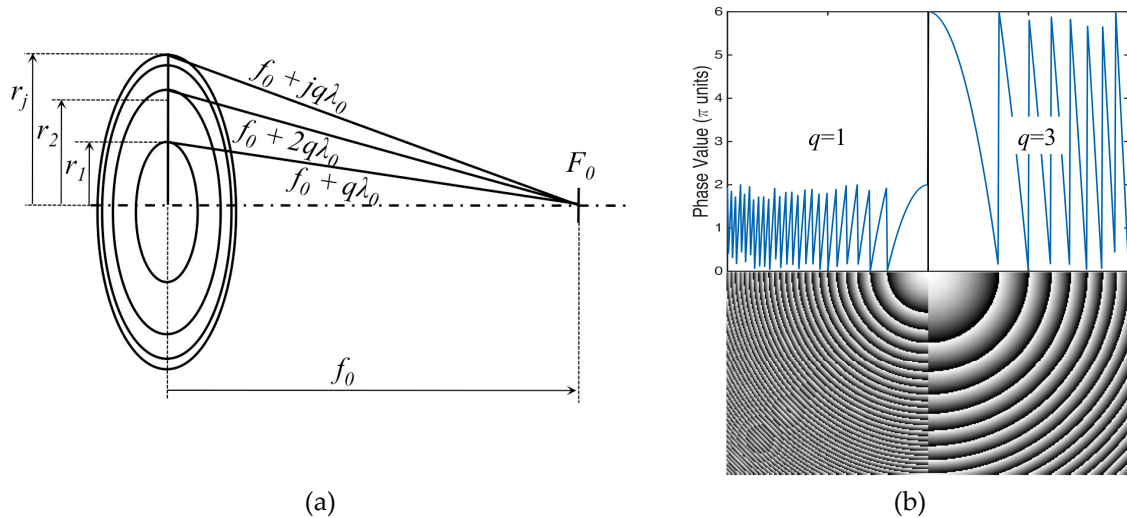


Figure 1. (a) Zone construction of a multiorder (q th-order) diffractive lens whose optical path difference (OPD) between consecutive zones is q integer times the design wavelength λ_0 . (b) Profiles for a diffractive lens with 2π rad ($q = 1$) and 6π rad ($q = 3$) phase modulation depths.

The condition for obtaining a constructive interference in the focal plane F_0 of the lens determines the radial position of the j th diffractive zone, which is computed through the Pythagorean theorem

$$r_j^2 = (f_0 + jq\lambda_0)^2 - f_0^2 \approx 2jq\lambda_0 f_0. \tag{1}$$

The maximum variation of the phase profile in each zone is given by $q2\pi$. The lens has an infinite number of focal lengths according to

$$f(\lambda) = \frac{q\lambda_0 f_0}{m\lambda}. \tag{2}$$

The interested reader is referred to [2] for a detailed explanation of how Equation (2) is obtained. Note that Equation (2) justifies the highly dispersive nature of diffractive lenses.

For a conventional modulo 2π diffractive lens ($q = 1$) illuminated with the design wavelength ($\lambda = \lambda_0$), an infinite number of focal planes $f = f_0/m$ exist for the different diffraction orders [8]. If one considers a multiorder diffractive lens ($q > 1$), the optical path length $q\lambda_0$ for the design wavelength may coincide with other wavelengths for which the phase change between adjacent steps of the lens is a multiple of 2π . These wavelengths, which are called the resonant wavelengths [1], fulfill $\lambda = q\lambda_0/m$, and have a common focal plane $f(\lambda) = f_0$.

Not only does the location of the focal plane coincide for the resonant wavelengths but also the diffraction efficiency of the respective diffraction orders, which is given by [4]

$$\eta_{m,q} = \text{sinc}^2(\alpha q - m). \tag{3}$$

Coefficient α is a wavelength detuning factor that can be approximated by $\alpha = \lambda_0/\lambda$ when low-dispersive materials, or even no dispersion, are considered. The maximum diffraction efficiency $\eta_{m,q} = 1$ is achieved for resonant wavelengths at their common focal plane of a multiorder diffractive lens. For first-order diffractive lenses with $q = 1$, all the energy concentrates on the first diffraction order ($m = 1$) with a quick but smooth decrease of the efficiency for wavelengths that differ from the design wavelength. As the phase profile increases its modulation range, that is, when $q > 1$,

resonant wavelengths get closer in the spectrum, and diffractive lenses of higher orders can be obtained; however, their diffracted intensity drops even faster with wavelength [4].

3. Liquid Crystal on Silicon (LCoS) Calibration Procedure and Phase Modulation Responses

We have used a parallel-aligned nematic LC device of LCoS-SLM technology from Holoeye (Pluto-BB-HR, HOLOEYE Photonics AG, Berlin, Germany) with 1920×1080 pixels of size $8 \times 8 \mu\text{m}^2$, fill factor of 87%, and refreshing rate of 60 Hz. This device is a phase-only SLM working on a reflective mode. An achromatic half-wave plate with a nearly flat retardance over the operation range (400–800 nm) from Thorlabs (AHWP05M-600, Thorlabs GmbH, Dachau/Munich, Germany) was used to adjust the polarization plane of the incident beam from a tunable Ar ion linearly polarized laser (35KAP431, Cvi Melles Griot, Inc., Albuquerque, New Mexico, USA) to obtain a phase-only modulation output. Normal incidence of the impinging collimated beam combined with the use of a beam splitter was chosen to assure an optimal response of the LCoS display in terms of phase modulation depth and negligible depolarization [12].

Characterization of the LCoS device was carried out to assure an optimal implementation of multiorder diffractive lenses. The procedure was done by means of the Michelson interferometer with coherent illumination shown in Figure 2. A broadband hybrid metal dielectric coating cube beamsplitter (03BSC009, Cvi Melles Griot, Inc., Albuquerque, New Mexico, USA) (BS in Figure 2) that exhibits little polarization sensitivity for the 450–700 nm spectral range was used in the setup to assure that it did not significantly affect the linear polarization state of incident beams. A flat mirror slightly tilted with respect to the SLM plane permitted us to obtain an interferogram pattern of the two beams consisting of a set of vertical fringes. The corresponding interferogram was acquired with a charged coupled device (CCD) camera (pco.1600, PCO AG, Kelheim, Germany) with 1600×1200 pixel resolution and 14 bit dynamic range (Figure 3a).

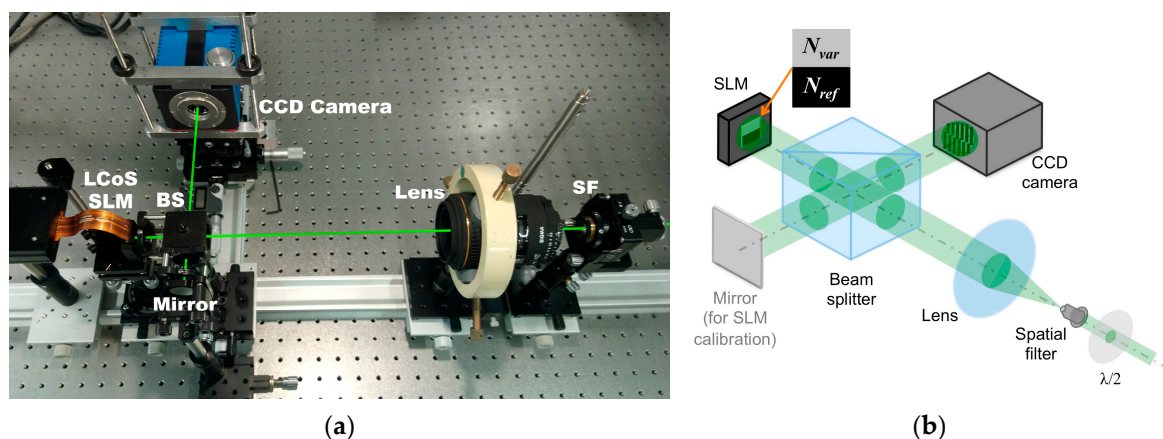


Figure 2. (a) Michelson interferometer setup for characterization of the LCoS display (BS stands for beam splitter and SF for spatial filter). The tunable linearly polarized Ar ion-laser and the half-wave plate are not shown. (b) Scheme of the Michelson interferometer with a detailed view of the spatial light modulator (SLM) input plane.

The SLM screen was divided in two uniform sectors, one half with a constant grey level kept as a reference and the other half with a varying uniform grey level among the 256 grey levels available (Figure 2b). The fringe shift between the two sectors allowed us to calculate the phase variation for each grey level (Figure 3a). The procedure is described with more detail in ref. [13].

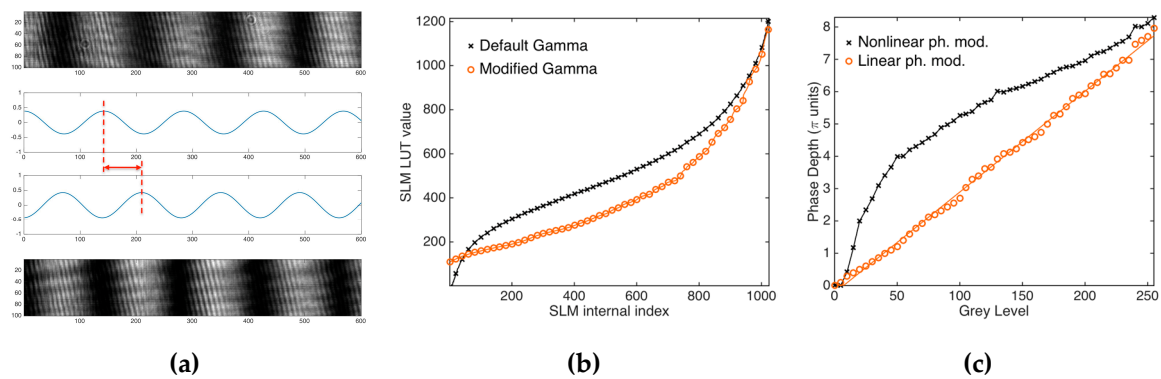


Figure 3. (a) Interferogram obtained when two different gray levels are sent to the top and bottom halves of the SLM display (Figure 2b). The phase difference is measured from the detected fringe shift. (b) Look-up tables (LUTs), also named gamma curves, to control the response of the SLM display and (c) measured phase modulation depth. Line curves with cross markers from (b,c) correspond to the initial measurement when the gamma curve provided by the manufacturer is used (default gamma). The corresponding phase modulation slightly exceeds 8π radians but with a nonlinear response. Line curves with circles from (b,c) correspond to the modified gamma curve that achieves a linear phase modulation of the display. The LCoS display was illuminated with $\lambda_G = 514$ nm.

Calibration curves were obtained for different configuration conditions of the SLM display in order to optimize the configuration parameters to achieve a variety of phase modulation ranges. The Holoeye modulator is electrically addressed by means of a standard digital video interface (DVI) connector and works with two bit-plane configurations (5-5 and 18-6), which allow mapping the 256 video grey levels to either 192 or 1216 index levels of the look-up table (LUT), respectively, loaded in the hardware of the device. Even though the number of addressable values for the 5-5 bit-plane profile is lower, this configuration is intended to reduce the flickering effects of the display. For this reason, the 5-5 bit-plane scheme was the chosen configuration for the calibration of the device, except for the case of the maximum 8π phase modulation, which was only achieved by the 18-6 bit-plane profile. Initially, the LUT (also named gamma curve) provided by the SLM manufacturer (“default gamma”, curve with cross markers in Figure 3b) was used to control the display. Two electronic potentiometers were properly adjusted to obtain a given device response. By modifying the varying grey level among the 256 grey values, the phase modulation response was measured (“nonlinear ph. mod.”, line with cross markers in Figure 3c). From this measurement, a new LUT was established (“modified gamma”, line with circles in Figure 3b) in order to achieve a linear phase modulation (“linear ph. mod.”, line with circles in Figure 3c). Figure 3 depicts the modified LUT and the corresponding linear performance for up to 8π phase modulation range for an illuminating wavelength of $\lambda_G = 514$ nm. In this condition, we measured the response of the display for another wavelength in the green region of the spectrum, $\lambda_G = 520$ nm (Figure 4). Note that the SLM phase modulation response with the new calibration LUT (or modified gamma curve) does not vary remarkably when a different, but close, illuminating wavelength is used. Thus, we assume that the phase modulation response is resistant to slight variations in the illuminating wavelength with respect to the one used to determine the new gamma curve.

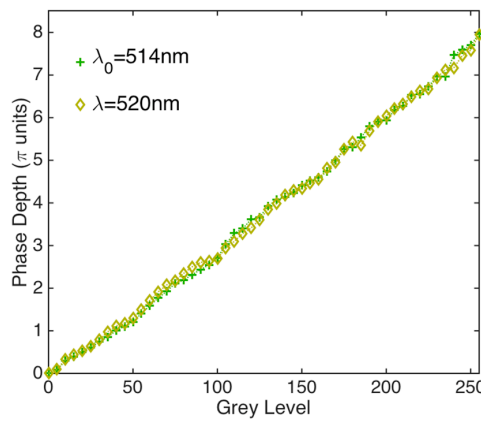


Figure 4. Phase modulation of the LCoS for two green wavelengths $\lambda_0 = 514 \text{ nm}$ (used in the characterization) and $\lambda = 520 \text{ nm}$ when the SLM display operates with the LUT that linearizes the 8π phase modulation range for $\lambda_0 = 514 \text{ nm}$ (Figure 3b,c).

Next, we measured the light reflected by the SLM display when a uniform image of a varying grey level was depicted as a full screen on the display. Light coming from the flat mirror was blocked at this time. The CCD camera was replaced by a photodetector so that the detector cell received the light reflected from the SLM display and integrated it. Figure 5a sketches the setup, and Figure 5b shows the modulation detected on the reflected light for the three illuminating wavelengths used sequentially in this experiment. This effect is due to the Fabry–Perot interference on the round-trip propagation inside the liquid crystal layer as already described in Refs. [6,14]. The number of oscillations in each plot accounts for the corresponding phase modulation range that approximates 6π , 8π , and 9π for $\lambda_R = 647 \text{ nm}$, $\lambda_G = 514 \text{ nm}$, and $\lambda_B = 476 \text{ nm}$, respectively. As shown in Figure 4b, the experimental results obtained with our LCoS-SLM are in very good agreement with those reported by Calero et al. for another LCoS-SLM device (Hamamatsu X10468-08) [6].

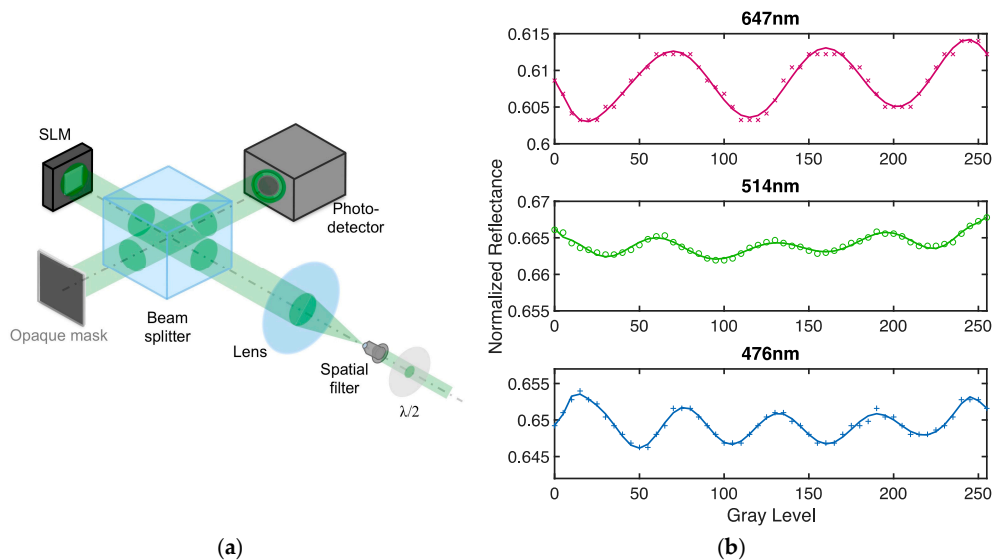


Figure 5. (a) Scheme of the experimental setup. (b) Reflectance modulation versus varying grey level addressed to the SLM.

We were able to obtain a variety of linear phase modulation ranges, from π up to 8π , by properly setting the configuration parameters of the SLM control driver. In particular, optimized calibration curves were obtained for π , 2π , 3π , 4π , 6π , and 8π phase modulation ranges. An analogous calibration procedure was followed in all cases. For those calibration tasks, the illuminating wavelength was set

to 530 nm, which coincided with the maximum intensity of an available green LED source that was going to be used in subsequent experiments (display of Fresnel diffraction lenses). Once the calibration LUT was established, measurements for 647 and 476 nm, as representative of the available red and blue LED sources, were also taken.

From the plots of Figure 6, we remark that the phase modulation ranges were clearly linear as expected for the green source in all cases, and the phase modulation increases for shorter wavelengths because of the inverse dependence of the phase modulation with wavelength.

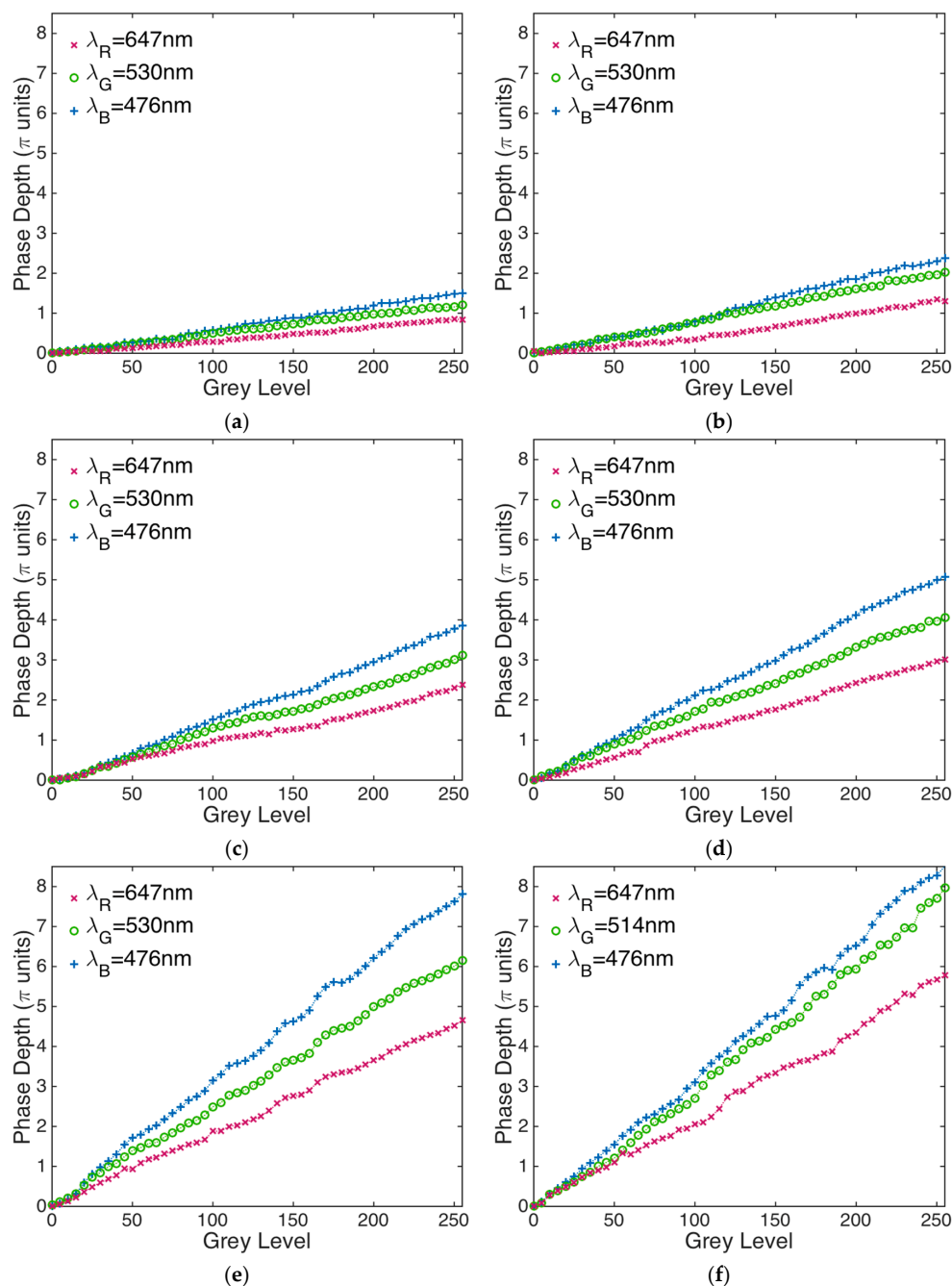


Figure 6. Phase modulation responses of the LCoS display for three different wavelengths ($\lambda_R = 647$ nm, $\lambda_G = 530$ nm, and $\lambda_B = 476$ nm). The calibration curves were optimized for $\lambda_G = 530$ nm and the phase modulation ranges: (a) 1π ; (b) 2π ; (c) 3π ; (d) 4π ; and (e) 6π while using the more stable SLM 5-5 bit-plane configuration. Note that the calibration curve for 8π phase modulation (f) was originally optimized for $\lambda_G = 514$ nm using the SLM 18-6 bit-plane configuration.

4. Overcoming the Nyquist Limit for a Lens with Low F-Number

Conventional modulo 2π diffractive lenses, which entail phase jumps of 2π for the design wavelength on either side of each zone boundary (Figure 1b), are designed to work efficiently in the first diffractive order [3,4]. One of the problems with the phase profile of a diffractive lens is that the phase function changes very rapidly at the outer part of the lens aperture. Thus, implementation is prone to undersampling and aliasing effects when the lens is displayed on a pixelated device (see, for instance, the bottom left corner of Figure 1b). As a rule of thumb, the range of focal lengths must meet the condition $f_N < f < 50f_N$. The inferior limit is the Nyquist focal length [7,11], which is given by

$$f_N = \frac{N\Delta^2}{\lambda}, \quad (4)$$

where Δ is the pixel pitch, and $N \times N$ is the size of the pixel array. Multiorder diffractive lenses with phase echelettes higher than modulo 2π (see Figure 1b) may overcome the limitations to implement first-order lenses. In that sense, new LCoS displays with large dynamic ranges in phase modulation offer advantages in comparison to older SLM technology.

If a first-order lens is displayed on a square area of $N = 1000$ pixels of the Holoeye LCoS SLM ($\Delta = 8$ microns pixel pitch) and is illuminated with $\lambda = 530$ nm, the corresponding Nyquist focal length—as derived from Equation (4)—will result in $f_N = 120$ mm (or equivalently, an optical power of 8.3 diopters). Thus, undersampling problems will arise at the periphery of the aperture if one implements a lens of shorter focal length (or higher optical power) on the display operating at a phase modulation range modulo 2π . In consequence, aliasing effects and poor performance would result. Let us overcome this situation by designing multiorder diffractive lenses.

Let us suppose we want to implement a diffractive lens with $f_0 = 80$ mm focal length (or, equivalently, 12.5 diopters). Note that $f_0 < f_N$ for the Holoeye LCoS-SLM. A possible solution would be to design a second-order lens of $f = 160$ mm that would obtain maximum efficiency on its second diffraction order located at $f/2 = f_0 = 80$ mm. Similarly, a third-order lens of $f = 240$ mm would concentrate the vast majority of the energy on its third diffraction order at $f/3 = f_0 = 80$ mm. Both multiorder diffraction lenses would have larger phase jumps at their edges in comparison to the conventional modulo 2π lens, and, in addition, both focal lengths (160 and 240 mm) would be above the Nyquist limit. Under these circumstances, the performances of second- and third-order lenses can be superior in comparison to conventional diffractive lenses.

We experimentally compared the performance of both multiorder lenses with their equivalent modulo 2π lens. We first considered a conventional lens with $f_0 = 80$ mm focal length for a design wavelength $\lambda_0 = 530$ nm. We displayed it on the LCoS display with the linear 2π calibration (Figure 6b) obtained for such wavelength. Note that the focal length of this lens is shorter than the focal length corresponding to the Nyquist limit ($f_N = 120$ mm), so that undersampling of the lens function will appear at the periphery of the lens. To avoid aliasing, we proposed a multiorder lens with larger focal length ($f > f_N$). We compared the performance of such a conventional lens with two different multiorder diffraction lenses: a second-order lens with $f = 160$ mm and a third-order lens with $f = 240$ mm computed for the design wavelength $\lambda_0 = \lambda_G = 530$ nm. The second-order diffraction lens was displayed on the LCoS by using the calibration LUT for a linear 4π phase variation (Figure 6d), whereas we implemented the third-order diffraction lens by using the linear 6π phase variation curve (Figure 6e) for the same design wavelength $\lambda_0 = \lambda_G = 530$ nm. Theoretically, all three lenses would have a common focalization plane at $f_0 = 80$ mm with 100% efficiency on its corresponding order of diffraction (first-order for the conventional modulo 2π lens, second-order for the modulo 4π lens, and third-order for the modulo 6π lens).

The setup sketched in Figure 7 was used in this experiment. It is similar to the Michelson interferometer used for characterization (Figure 2) but with some variations. In this experiment, a green LED source ($\lambda_G = 530$ nm) and a 100 micron pinhole were used to illuminate the setup, and a polarizer served to select the correct polarization plane of the light beam incident onto the SLM display.

Only the SLM arm was operative since light coming from the mirror was blocked with an opaque mask. And, finally, a microscope objective was attached to the CCD camera in order to acquire the focalization spots at the focal planes with appropriate magnification. This configuration, already used for device characterization, assures good control of the phase modulation for the on-axis operating lenses of our experiment (in the case of off-axis illumination with incident angle deviations within ± 10 degrees, no substantial changes in the modulation properties would be expected either [12]). The three aforementioned diffractive lenses were sequentially displayed on the SLM screen, and the obtained experimental results are summarized in Figure 8. Figure 8a depicts the profile of the focalization spots located at $f_0 = 80$ mm for the three analyzed lenses. Profiles are cropped so that only the central area of the output zoomed plane is plotted.

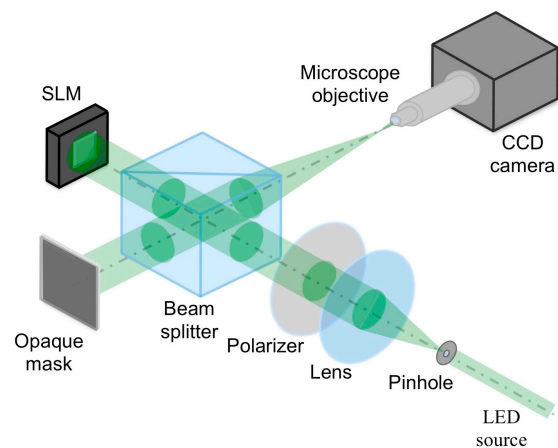


Figure 7. Setup for diffractive lens evaluation. Illumination is done with an LED source and a 100 micron pinhole. A polarizer selects the appropriate incidence on the SLM display. A microscope objective is attached to the charged coupled device (CCD) camera to capture the focal planes. Light coming from the mirror was blocked with an opaque mask.

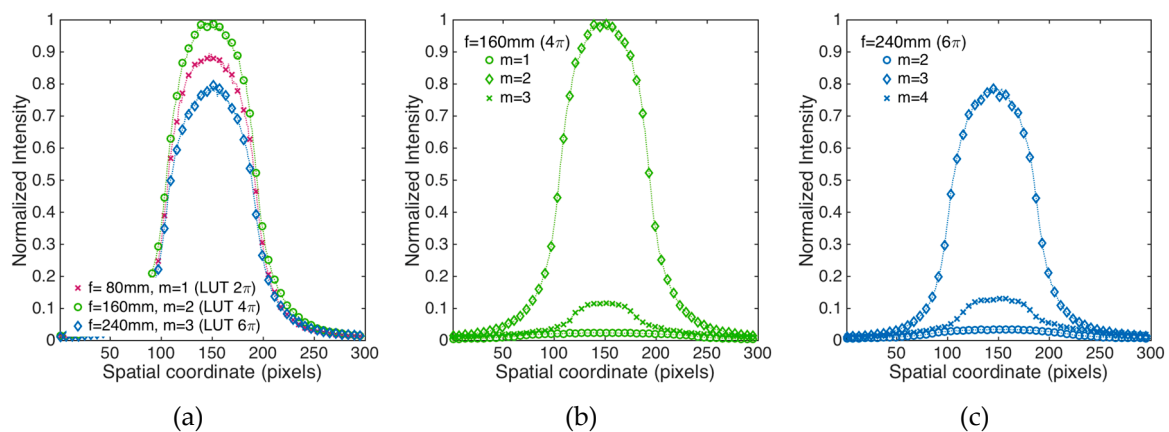


Figure 8. (a) Coincident focalization planes at $f_0 = 80$ mm for first-, second-, and third-order diffraction lenses. Calibrations curves for the linear 2π (Figure 6b), 4π (Figure 6d), and 6π (Figure 6e) responses were used, respectively. Different diffraction orders, at different locations, for (b) the second-order diffraction lens with $f = 160$ mm and (c) the third-order diffraction lens with $f = 240$ mm.

Intensity profiles plotted in Figure 8 were normalized to the maximum intensity peak obtained for the modulo 4π lens. As expected, the second-order lens produced a more intense focalization spot than the conventional modulo 2π lens, since the latter was below the Nyquist limit to reproduce the smallest details at the edges of the lens, whereas the modulo 4π lens avoided the aliasing effect. According to the graph, the focal spot of the modulo 2π lens was affected by an intensity reduction of about 10%

with respect to the modulo 4π lens. In the same Figure 8a, the intensity profile for the modulo 6π lens showed that this diffractive lens obtained the lowest focalization peak. It experienced a reduction around 20% of the maximum intensity. A possible reason for the latter result can be the fact that the LCoS display has a maximum of 256 grey levels to address the diffractive optics. The same number of grey levels is used to reproduce a phase range of 4π and 6π , so that the second-order lens can be implemented more precisely, in particular, at the central part of the lens aperture compared to the coarser reproduction of the third-order lens. Thus, the third-order lens would have larger quantization error than the second-order lens.

Figure 8b,c show the profiles of diffraction orders other than the one with a maximum efficiency for both the second-order lens and the third-order lens, respectively. In both cases, there was a small amount of light going to these orders, and both multiorder lenses had similar behaviors.

A second experiment was carried out to show the importance of using the optimized characterization curve in each case and to test the effect of the quantization error on the implementation of the lenses. The three different lenses were now displayed on the LCoS SLM by using a single calibration curve: the one corresponding to a linear 6π phase variation (Figure 6e). In this situation, only the full 256 grey level range was available to encode the 6π phase modulation of the third-order diffraction lens, whereas only parts of it were effectively used to encode the 4π phase modulation of the second-order diffraction lens (166/256 grey levels) or the 2π phase modulation of the first-order diffraction lens (just 66/256 grey levels). Figure 9 plots the profiles of the corresponding diffraction orders. They are all normalized to the maximum intensity peak shown in Figure 8a for the sake of comparison.

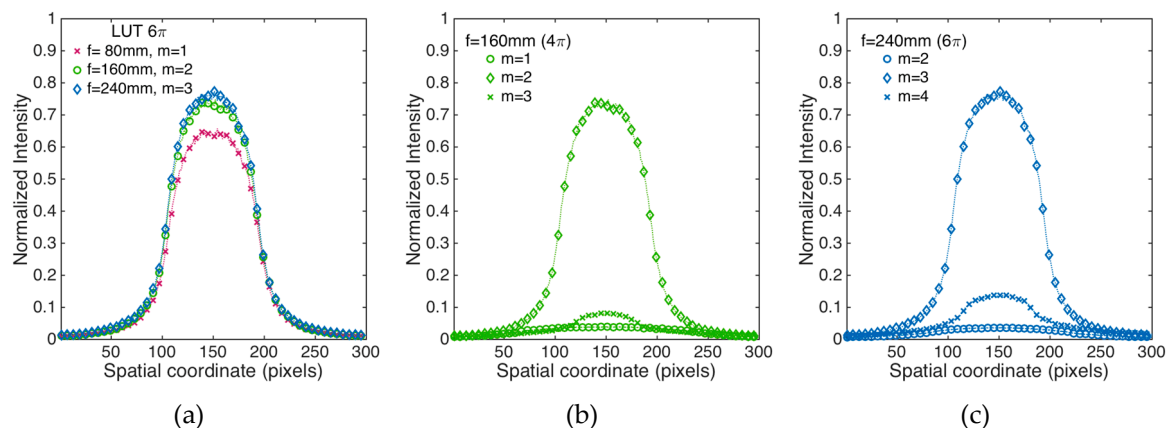


Figure 9. (a) Coincident focalization planes at $f_0 = 80$ mm for first-, second-, and third-order diffraction lenses when the 6π calibration curve (Figure 6e) is used in all the cases. Different diffraction orders, at different locations, for (b) the second-order diffraction lens with $f = 160$ mm and (c) the third-order diffraction lens with $f = 240$ mm.

In the analyzed situation, the most intense focalization peak was obtained for the third-order lens because its profile—with greater rings corresponding to a longer focal length and bigger facets at the periphery—could be encoded with the full grey level range. A slightly less intense peak (less than 5% of intensity reduction) was obtained for the second-order lens, mainly because it had a reduced number of phase levels (166 grey levels) to encode the 4π phase modulation. The focalization peak obtained for the conventional 2π lens had the lowest intensity among the profiles depicted in Figure 9a. The intensity reduction was around 15% compared to the third-order diffractive lens with full grey level range. The poor performance of the first-order lens can mainly be due to the combination of aliasing at the boundaries of the lens and the quantization error produced for the even more limited number of grey levels available.

Figure 9b,c show the different diffraction orders obtained at different planes for both multiorder lenses. In this case, when both lenses were displayed on the LCoS screen with the same calibration curve, which corresponds to 6π phase modulation, they obtained very similar results.

The results of Figures 8a and 9a lead us to remark the importance of using an optimized SLM calibration curve to display DOEs. For instance, the performance of both the modulo 4π lens with only 166 grey levels and the modulo 2π lens displayed with only 66 grey levels (Figure 9a) experienced an intensity reduction of about 25% with respect to the same lenses implemented with the full grey level range (Figure 8a).

5. Experimental Achromatic Diffractive Lens Implemented in an LCoS Display

In this section, we show the potential of multiorder lenses displayed on an LCoS-SLM with a large phase dynamic range to design achromatic diffractive lenses. In the exemplary study of this section, we considered a diffractive lens of 150 mm focal length under polychromatic illumination. The described Holoeye LCoS display permits a maximum phase modulation range of 8π (Figures 4 and 6f) for a wavelength in the green region of the visible spectrum (514, 520 nm), attaining a larger phase modulation depth in the blue region (476 nm) and approaching 6π in the red region (647 nm). By using the response curves of Figure 6f, we designed a four-order diffractive lens for a design wavelength $\lambda_0 = 470$ nm and $f = 600$ mm focal length that operates with maximum efficiency in its fourth diffraction order at $f/m = 600/4 = 150$ mm. This four-order diffractive lens under blue illumination has a phase profile that behaves, under illumination with $\lambda_R = 625$ nm, as a third-order diffractive lens of $f = 450$ mm that shows its maximum diffraction efficiency at $f/m = 450/3 = 150$ mm from the lens plane (Equations (2) and (3)). In other words, such a phase profile achromatizes the multiorder diffractive lens with a common plane of maximum efficiency for both the blue and red wavelengths.

We compared the performance of this multiorder lens, designed to be ideally achromatic, with a conventional modulo 2π lens, designed for $\lambda_0 = 530$ nm with a focal length $f_0 = 150$ mm, when both were illuminated under polychromatic light. These lenses were implemented on the LCoS display using either the calibration curve for a linear 8π phase modulation (Figure 6f) (achromatic multiorder lens) or the calibration curve for a linear 2π phase modulation (Figure 6b) (conventional modulo 2π lens). The setup depicted in Figure 7 was used in this experiment. We sequentially illuminated both lenses with three different LED sources whose featured wavelengths covered the visible spectrum ($\lambda_B = 470$ nm, $\lambda_G = 530$ nm, and $\lambda_R = 625$ nm) and acquired the focal spots at the planes of higher diffraction efficiency. Distance from the LCoS screen was measured in each case.

Figure 10 shows the experimental results. Figure 10a shows the focalization planes obtained for the conventional modulo 2π diffractive lens. At the location of the design focal plane ($f_0 = 150$ mm) the focal spot for the green LED ($\lambda_G = 530$ nm) was obtained. When the first-order diffractive lens was illuminated with either the red or blue LEDs, the focal plane moved in opposite direction with respect to the green wavelength. Both red and blue focal plane positions are indicated in Figure 10a. These results evidence the remarkable chromatic aberration of a diffractive lens, for which focal planes for the three R, G, and B testing wavelengths are located some distance apart from each other. In our experiment, the focal planes of the extreme wavelengths of the visible spectrum (625 and 470 nm) are separated around 41 mm.

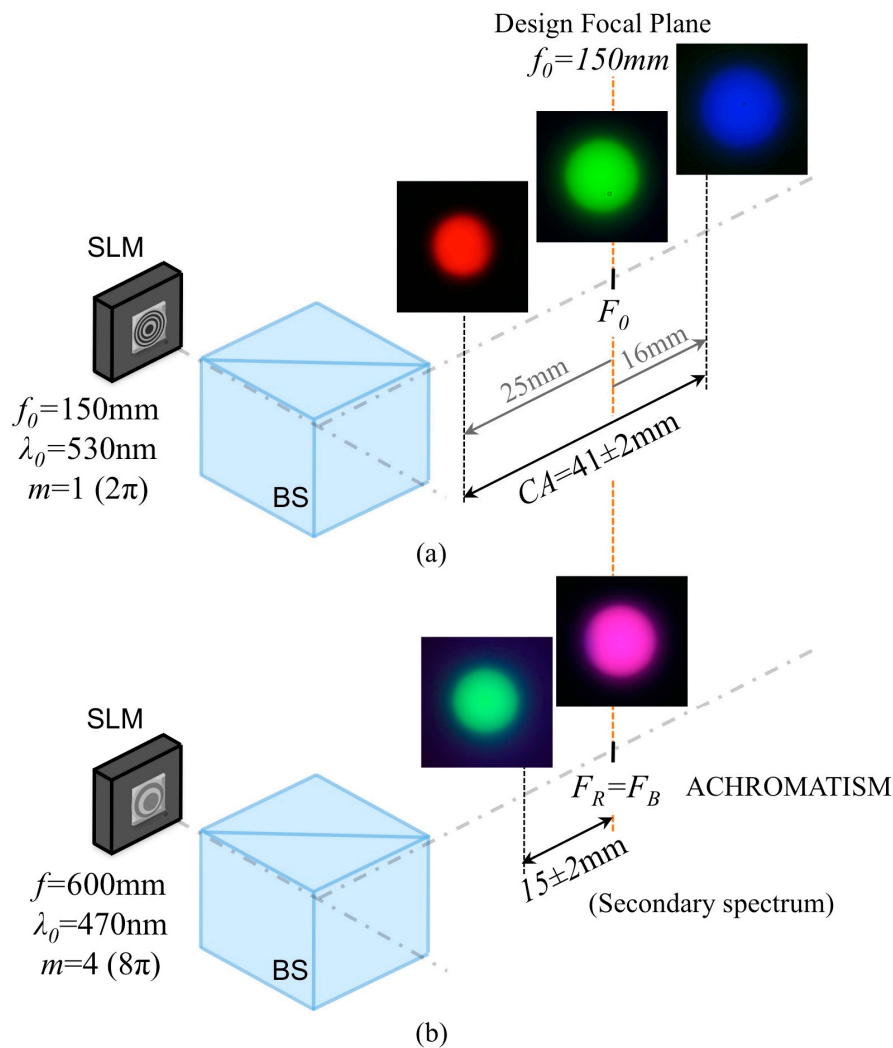


Figure 10. Experimental results for (a) Conventional modulo 2π diffractive lens for $\lambda_0 = 530\text{ nm}$ and $f_0 = 150\text{ mm}$ sequentially illuminated with three different wavelengths $\lambda_R = 625\text{ nm}$, $\lambda_C = 530\text{ nm}$, and $\lambda_B = 470\text{ nm}$. The focalization planes with the maximum diffraction efficiencies are shown at the location where they were acquired. (b) Analogous results for a fourth-order modulo 8π diffractive lens for $\lambda_0 = 470\text{ nm}$ and $f = 600\text{ mm}$ that worked in its fourth diffraction order located at $f/m = 600/4 = 150\text{ mm}$.

Figure 10b provides the experimental results for the achromatic multiorder lens. It consists of a fourth-order diffractive lens with a $f = 600\text{ mm}$ focal length for a design wavelength of $\lambda_0 = \lambda_B = 470\text{ nm}$. The lens was sequentially illuminated by the three LED sources in the red, green, and blue regions of the visible spectrum. Focalization planes with the highest diffraction efficiencies were acquired, and their positions from the LCoS screen were measured. As a fourth-order diffractive lens ($m = 4$) for the blue light, the focalization plane with maximum efficiency for blue was located at $f/m = 600/4 = 150\text{ mm}$ from the SLM display. Since this lens was, at the same time, a third-order diffractive lens for red light ($\lambda_R = 625\text{ nm}$), both bright blue and red spots appeared at the same position. The intensity spots captured by the CCD camera as well as their relative distances from the desired focal plane at 150 mm are shown in Figure 10b. These results demonstrate that the design multiorder lens has a resonant wavelength in the red region of the visible spectrum. Thus, for both wavelengths, $\lambda_0 = \lambda_B = 470\text{ nm}$ and $\lambda_R = 625\text{ nm}$, the lens has a common focus at $f_0 = 150\text{ mm}$, which constitutes an achromatic lens. The light from the green LED, which is approximately in the middle of the spectrum, “sees” the diffractive lens with intermediate phase modulation steps, and the maximum intensity is obtained

in a plane located 15 mm apart from the common red and blue foci. Thus, the secondary spectrum (residual chromatic aberration) for this multiorder lens drops to around one-third of the chromatic aberration measured for the conventional lens shown in Figure 10a.

6. Conclusions

A thorough characterization of a LCoS SLM display (Holoeye-Pluto-BB_HR) working on reflection has been carried out to obtain the optimized LUT curves for achieving different phase modulations, ranging from π up to 8π . Wavelengths from the green region of the visible spectrum (514, 520, and 530 nm) have been used to measure the various phase variation ranges and to compensate for some nonlinearities of the SLM response. From these initial measurements, the corresponding LUT curves were determined so that π , 2π , 3π , 4π , 5π , 6π , and 8π phase ranges were linearly reproduced by the SLM device. By using these phase modulation ranges, a number of multiorder diffractive lenses were displayed on the SLM device, and their performances were compared experimentally with the results of a conventional first-order diffractive lens. Second- and third-order diffractive lenses have proved to be very useful to overcome the undersampling problems raised when encoding a lens of relatively low f-number or optical power exceeding the Nyquist condition.

We have also shown the benefits of determining optimized LUT curves for each phase modulation range, since DOE performance exhibits better optical quality when the appropriate LUT with a full grey level range is used. According to the results obtained for high-order diffractive lenses, it is also preferable to have a sufficient range of available grey levels to smoothly display the phase function.

The so-obtained optimized LUT curves were used to determine the LCoS-SLM response for extreme wavelengths of the visible spectrum in the blue and the red regions. This information permitted the design of an achromatic, multiorder lens with a residual chromatic aberration reduced to one-third of the chromatic aberration of a conventional first-order diffractive lens. A fourth-order lens design for a blue wavelength ($\lambda_0 = 470$ nm) has a common focalization spot when it operates as a third-order diffractive lens for the red illumination wavelength $\lambda_R = 625$ nm, as demonstrated experimentally by our results.

Author Contributions: Conceptualization, methodology, validation, formal analysis, investigation, resources and writing—review and editing, M.S.M. and E.P.-C.; software, data curation and writing—original draft preparation, E.P.-C.; project administration and funding acquisition, M.S.M.

Funding: This research was funded by the Spanish Ministerio de Economía y Competividad and FEDER Funds (ref. DPI2016-76019-R).

Acknowledgments: Authors thank José Valverde and Joan Goset for their contribution in the experimental LCoS calibration procedure.

Conflicts of Interest: The authors declare no conflict of interest.

References

1. Sweeney, D.W.; Sommargren, G.E. Harmonic diffractive lenses. *Appl. Opt.* **1995**, *34*, 2469–2475. [[CrossRef](#)] [[PubMed](#)]
2. Faklis, D.; Morris, G.M. Spectral properties of multiorder diffractive lenses. *Appl. Opt.* **1995**, *34*, 2462–2468. [[CrossRef](#)] [[PubMed](#)]
3. Turunen, J.; Wyrowski, F. *Diffractive Optics for Industrial and Commercial Applications*, 1st ed.; Akademie Verlag (Wiley-Vch.): Berlin, Germany, 1997.
4. O’Shea, D.C.; Suleski, T.J.; Kathman, A.D.; Prather, D.W. *Diffractive Optics Design, Fabrication and Test*, 2nd ed.; Tutorial Texts in Optical Engineering; SPIE Press: Bellingham, WA, USA, 2015; Volume TT62.
5. Albero, J.; García-Martínez, P.; Martínez, J.L.; Moreno, I. Second order diffractive optical elements in a spatial light modulator with large phase dynamic range. *Opt. Lasers Eng.* **2013**, *51*, 111–115. [[CrossRef](#)]
6. Calero, V.; García-Martínez, P.; Albero, J.; Sánchez-López, M.M.; Moreno, I. Liquid crystal spatial light modulator with very large phase modulation operating in high harmonic orders. *Opt. Lett.* **2013**, *38*, 4663–4666. [[CrossRef](#)] [[PubMed](#)]

7. Cottrell, D.M.; Davis, J.A.; Hedman, T.R.; Lilly, R.A. Multiple imaging phase-encoded optical elements written as programmable spatial light modulators. *Appl. Opt.* **1990**, *29*, 2505–2509. [[CrossRef](#)] [[PubMed](#)]
8. Moreno, I.; Iemmi, C.; Márquez, A.; Campos, J.; Yzuel, M.J. Modulation light efficiency of diffractive lenses displayed in a restricted phase-mostly modulation display. *Appl. Opt.* **2004**, *43*, 6278–6284. [[CrossRef](#)] [[PubMed](#)]
9. Arrizón, V.; Carreón, E.; González, L.A. Self-apodization of low-resolution pixelated lenses. *Appl. Opt.* **1999**, *38*, 5073–5077. [[CrossRef](#)] [[PubMed](#)]
10. Yzuel, M.J.; Campos, J.; Márquez, A.; Escalera, J.C.; Davis, J.A.; Iemmi, C.; Ledesma, S. Inherent apodization of lenses encoded on liquid-crystal spatial light modulators. *Appl. Opt.* **2000**, *39*, 6034–6039. [[CrossRef](#)] [[PubMed](#)]
11. Millán, M.S.; Otón, J.; Pérez-Cabré, E. Chromatic compensation of programmable Fresnel lenses. *Opt. Express* **2006**, *14*, 6226–6242. [[CrossRef](#)] [[PubMed](#)]
12. Lizana, A.; Martín, N.; Estapé, M.; Fernández, E.; Moreno, I.; Márquez, A.; Iemmi, C.; Campos, J.; Yzuel, M.J. Influence of the incident angle in the performance of Liquid Crystal on Silicon displays. *Opt. Express* **2009**, *17*, 8491–8505. [[CrossRef](#)] [[PubMed](#)]
13. Otón, J.; Ambs, P.; Millán, M.S.; Pérez-Cabré, E. Multipoint phase calibration for improved compensation of inherent wavefront distortion in parallel aligned liquid crystal on silicon displays. *Appl. Opt.* **2007**, *46*, 5667–5679. [[CrossRef](#)] [[PubMed](#)]
14. Davis, J.A.; Tsai, P.; Cottrell, D.M.; Sonehara, T.; Amako, J. Transmission variations in liquid crystal spatial light modulators caused by interference and diffraction effects. *Opt. Eng.* **1999**, *38*, 1051–1057. [[CrossRef](#)]



© 2019 by the authors. Licensee MDPI, Basel, Switzerland. This article is an open access article distributed under the terms and conditions of the Creative Commons Attribution (CC BY) license (<http://creativecommons.org/licenses/by/4.0/>).